Journal of Applied Fluid Mechanics, Vol. 16, No. 11, pp. 2263-2276, 2023.
Available online at www.jafmonline.net, ISSN 1735-3572, EISSN 1735-3645.
https://doi.org/10.47176/jafm.16.11.1799

Numerical Investigation of Optimal Hydrodynamic Performance by Changing the Orifice Ratio and Relative Opening of a Land-Fixed Rectangular-based OWC

S. Ranjan and P. DebRoy†

Department of Mechanical Engineering, NIT, Silchar, Assam - 788 010, India

†Corresponding Author Email: pdebroy@mech.nits.ac.in

ABSTRACT

The energy that can be extracted from the ocean is inexhaustible. An oscillating water column (OWC) is a wave energy converter that extracts this energy. A numerical investigation has been conducted by altering relative opening (α) and orifice ratio (τ) to assess the maximal energy of a land-fixed rectangular-based OWC model in a nonlinear wave field. The power of OWC has also been evaluated by the wave steepness (H/L) alteration. The numeric analysis has been imposed to obtain the optimal power using Fluent software in a three-dimensional tank. Validation of the present numeric model's result correlates with the printed empirical data. The Finite Volume Method **(**FVM) solves RANS equations, and the relevant waves are generated at the inlet of the numerical tank by the inlet velocity approach. The efficiency (η) increases with relative openings (α) increase. The efficiency (η) decreases with wave steepness (H/L) increase. The η reaches the optimum shown in the study at H/L = 0.02 and τ = 1.03% for entire values of α. The excellent energy of around 71.3% is attained at α =75% and H/L = 0.02. This study is a highly relevant source of information that finds the optimal efficiency of a land-fixed rectangular base OWC and gives prior knowledge of the performance of OWC before the real-life experiment.

Article History

Received February 5, 2023
Revised July 12, 2023
Accepted July 12, 2023
Available online September 3, 2023

Keywords:

Numerical modeling
Land-fixed OWC
Orifice ratio
Relative opening
Optimal performance
Second-order Stokes wave

1. INTRODUCTION

The energy density of ocean waves is higher than that of other renewable energy sources like biomass, wind, solar, etc. (Pontes & Falcao, 2001; Pinson et al., 2012). This massive amount of energy is still untapped because of the intricate behavior of ocean waves, although thousands of prototype patent runs successfully. Nowadays, the use of this energy is rapidly developing in various countries. Various wave energy converters (WEC), like Tidal WEC, Pelamis WEC, Wave Dragon, OWC, etc., convert ocean kinetic energy into electrical power. Among these varieties of wave energy converters, Falcão and Henriques (2016) reviewed in detail by literature survey the mechanism of oscillating water columns and the use of well and impulse turbines in the OWC devices. The important issues in controlling the turbine's rotational speed by reactive phase control and phase control. Different scientists and researchers have proposed two types of this technology: fixed and floating. The fixed OWC device was developed by Whittaker et al. (1993) and Yu et al. (1997). The floating OWC device was developed by Washio et al. (2000) and Hotta et al. (1988). The present model is a land-fixed rectangular-based OWC device described to understand the performance of OWC under different wave steepness conditions. The system consists of a vertical water column with air in the upper section and seawater in the lower sections. The lower section is under the water and opens, through which water enters into the chamber. The free water's surface in the column begins to fluctuate due to the effect of ocean waves. This oscillation causes the air above the water in the chamber to be compressed and expanded and generate electrical power by converting mechanical energy (Fig. 1). Morris-Thomas et al. (2007). The performance study of this technology and its advantages are well-proven compared to the other concepts (e.g., absence of moving elements, reliability, structural simplicity).

The OWC device is still a general uncertainty due to inefficient design, which must be carefully addressed. The front wall or lip wall design is required to be carefully addressed. Ocean waves propagate toward shore and lose some power due to refraction, reflection, and diffraction from the lip wall while entering the water in the column (Malmo & Reitan, 1985, 1986). They have developed the

NOMENCLATURE

a	Opening height of the chamber	S_o	Cross-sectional area of the orifice
b	Length of the OWC device	S_w	Free surface area inside the OWC chamber
c	Orifice diameter	T	Time period
$C_{\mu}, C_{\varepsilon 1}$	Empirical coefficients	$\overline{V}$	Velocity vector
d	Water depth	$v(t)$	Free surface velocity inside the chamber
g	Acceleration due to gravity	w	Width of the OWC device
G_k	Turbulent energy production	$\Delta x, \Delta y, \& \Delta z$	Size of elements
H	Wave height	α	Relative opening
L	Wave Length	ε	Turbulence dissipation rate
l_h	Tank height	η	Hydrodynamic efficiency
l_t	Tank length	μ	Dynamic viscosity
l_{wg}	Wave generating zone	μ_t	Eddy viscosity
k	Wave number	ω	Angular frequency
k	Turbulence kinetic energy	ρ	Air-water mixture density
$\overline{p}$	Average pressure	ρ_a	Air density
P_{in}	Incident wave power	ρ_w	Water density
P_{out}	Output power	$\sigma_k, \sigma_{\varepsilon}$	Empirical coefficients
$p(t)$	Fluctuating pressure	τ	Orifice Ratio

lip wall design in their research. Whittaker and Stewart (1993) experimentally investigated OWC's performance wave power apparatus. They found proper power extraction from OWC is possible by correctly choosing the optimal damping. Evans and Porter (1995) investigated the hydrodynamic performances of OWC by changing geometrical parameters and ignoring lip wall thickness. Wang et al. (2002) studied the effects of the bottom slope along the coastline on the OWC's hydrodynamic efficiency wave energy device using analytical and experimental methods. At low frequencies, they found that the capture-width ratios were most strongly influenced by the bottom slope. The depth of the water also has a significant impact on hydrodynamic performance. Different researchers at the early stage have investigated different theoretical methods to understand the performance of hydrodynamic efficiencies of OWC devices, such as Falnes and McIver (1985); Evans (1982); McCormick (1976); Falcão and Sarmento (1980); Evans (1978). Most of the past researchers used linear wave theory to explain the performance of the wave energy mechanism OWC and neglected the viscous effect (Zhang et al., 2012; Ning et al., 2015). The efficiency of the OWC energy converter was studied by Count and Evans (1984) through the development of the 3D boundary integral approach (BIM). Utilizing the first-order boundary element method (BEM), Delauré and Lewis (2003) conducted a numerical study on the efficiency of oscillating water columns. Josset and Clément (2007) predicted the annual performance of the OWC power plant through field observation at Pico Island, Azores, Portugal. The optimal design is required to improve the performance of OWC by changing the chamber geometry and turbine damping (Luo et al., 2014; Pereiras, 2015). Many authors focused their research on different geometrical shapes of OWC to develop hydrodynamic efficiency. The present numerical model used ANSYS FLUENT software to investigate the efficiency of OWC and calibrate and validate it with the published experimental results Çelik and Altunkaynak (2019).

Computational fluid dynamics (CFD) is a sophisticated tool used in numerous studies to analyze the efficiency of OWC wave energy converters. The CFD tool is appropriate for physical modeling. EI Marjani et al. (2008) numerically studied the flow behavior in the OWC chamber using Ansys Fluent software to observe hydrodynamic performance. López et al. 2014 numerical investigation of OWC devices to calculate the damping by ANSYS FLUENT software by considering a viscous model based on RANS equations. Open FOAM software was utilized by Iturrioz et al. (2015) to evaluate the efficacy of 3D modeling of the OWC model, and the findings were verified using CFD simulations.

Several researchers conducted various experimental studies to understand the OWC's efficiency. The results of these experiments were confirmed numerically. Thiruvenkatasamy and Neelamani (1997) experimented with testing the effectiveness of the OWC, and they found that it was inversely related to wave steepness. Tseng et al. (2000) constructed an OWC model of scale 1/20 to extract wave energy. The front wall geometry of the OWC device affects the result of hydrodynamic performance (Morris-Thomas et al. 2007). After that, Gouaud et al. (2010) studied the physical model and validated it with numerical results. Most of the other authors experimentally and numerically investigated the efficiency of an OWC model (e.g., Liu, 2008; Dizadji & Sajadian, 2011). The influence of the various bottom shapes on the OWC's hydrodynamic performance was explored experimentally (Ashlin et al., 2016). The results were found to be rather interesting. According to the author's observations, the circular bottom shape is the most effective of the four different designs. Ning et al. (2016a) studied the physical model by changing the orifice scale, bottom slope, and wave motion in the air chamber. The numerical findings of Ning et al. (2016b), which were previously published, were used to verify the outcomes of the experiments. They observed opening ratio significantly influences efficiency. Çelik and Altunkaynak (2019) experimentally investigated the OWC's performance of WEC.

The results of a numerical study conducted by Simonetti et al. (2017) to determine the efficiency of the OWC in a wave energy converter are then verified against experimental data. Liu et al. 2016 experimentally investigated the performance of the impulse turbine damping effect of the air chamber of OWC. Their research aims to optimize the orifice plate shape parameters as the pressure drop occurs in the impulse turbine, and then chamber performance is predicted numerically. Further, Yadav and DebRoy (2022) used computational methods to study the stable linear wave that continues in shallow water.

A survey of the relevant literature reveals that previous studies have focused on modifying geometrical factors to examine the effects of hydrodynamic performance on both floating and fixed-type OWC devices. The former researchers studied the numerical OWC model and validated the results experimentally or mathematically. However, the design of the OWC devices is still undeveloped due to reflection from the lip wall while entering the water in the column, which must be carefully addressed. The effect of orifice ratio, relative opening, wave steepness, and relative depth requires a detailed study on the OWC that previous researchers have not discussed adequately. Previous researchers ignored the effect of lip wall shape on the performance of the wave energy converter OWC which has required a detailed study. Streamline motion of the wave is a critical study to understand the inhalation and exhalation of the air within the chamber that previous researchers have not studied adequately. Moreover, the water's oscillating motion within the chamber is insufficiently focused. The massive dissimilarity in water surface elevation within and outside the chamber can cause damage to the front wall of the OWC devices that must be addressed carefully.

The fundamental objective of this work is to determine the maximum performance of land-fixed rectangular OWC models and to statistically explore the consequence of orifice ratio, relative opening, wave steepness, and relative depth on hydrodynamic efficiency. A 3D model of the OWC devices was tested in an NWT to achieve this goal. Second-order wave theory was used to complete the test under five wave steepness conditions. The present study carefully addressed the performance of the OWC model on the free surface motion, pneumatic pressure distribution at the different instants of time, streamlined motion, and the vortex formation in front and behind the front wall of the air chamber. The present results are calibrated and validated by the published results of Çelik and Altunkaynak (2019).

This paper is organized as follows. In section 1, we systematically review the previous reports to identify the research gap in the present study. Section 2 discusses the governing equations of the numerical model concerning the flow field within the chamber using ANSYS FLUENT software. Section 3 explains the tank's geometry scientifically, followed by the geometry of the OWC. Sections 3.3 and 3.4 discuss the convergence test and model validation. Finally, section 4 summarised the hydrodynamic performance of the OWC device under different wave conditions. The paper ends with the concluding remarks in section 5.

2. MATHEMATICAL FORMULATION

2.1 Governing Equation

Governing equations are continuity and RANS equations used to solve the incompressible turbulence fluid.

$$\frac{\partial \bar{u}_i}{\partial x_i} = 0 \quad (i = 1,2,3) \tag{1}$$

$$\rho\left[\frac{\partial \bar{u}_i}{\partial t} + \bar{u}_j \frac{\partial \bar{u}_i}{\partial x_j}\right] = -\frac{\partial \bar{p}}{\partial x_i} + \frac{\partial}{\partial x_j}\left[\mu \frac{\partial \bar{u}_i}{\partial x_j} - \rho\overline{u_i' u_j'}\right] + \rho g_i \tag{2}$$

Where an additional term is $\rho\overline{u_i' u_j'}$. $\bar{u}_i$ and $\bar{p}$ are the average velocity and pressure, respectively. The subscripts i, j = 1, 2, 3 indicate three-dimensional components as (u, v, w) or (u_1, u_2, u_3) and (x, y, z) or (x_1, x_2, x_3). The turbulence viscosity k-ε model is used here.

$$\frac{\partial}{\partial t}(\rho k) + \frac{\partial}{\partial x_i}(\rho k \bar{u}_j) = \frac{\partial}{\partial x_j}\left[\left(\mu + \frac{\mu_t}{\sigma_k}\right)\frac{\partial k}{\partial x_j}\right] + \rho G_k - \rho\varepsilon \tag{3}$$

$$\frac{\partial(\rho\varepsilon)}{\partial t} + \frac{\partial}{\partial x_i}(\rho\varepsilon \bar{u}_j) = \frac{\partial}{\partial x_j}\left[\left(\mu + \frac{\mu_t}{\sigma_\varepsilon}\right)\frac{\partial \varepsilon}{\partial x_j}\right] + \frac{\varepsilon}{k}(c_{\varepsilon 1}\rho G_k - c_{\varepsilon 2}\rho\varepsilon) \tag{4}$$

$$\mu_t = \frac{c_\mu \rho k^2}{\varepsilon} \tag{5}$$

$$G_k = \frac{\mu_t}{\rho}\left(\frac{\partial \bar{u}_i}{\partial x_j} + \frac{\partial \bar{u}_j}{\partial x_i}\right)\frac{\partial \bar{u}_i}{\partial x_j} \tag{6}$$

Here, C_μ = 0.09; $C_{\varepsilon 1}$ = 1.44; $C_{\varepsilon 2}$ = 1.92; σ_k = 1.0; σ_ε = 1.3.

The governing equations are solved by the VOF method at the interface of the two immiscible fluids simultaneously (Hirt & Nichols, 1981). The VOF method simulates two-phase flow. There are three possible circumstances, f_i = 1 means the cell contains water, and f_i = 0 means the cell contains air. The interface represents 0 < f_i < 1. Therefore,

$$\frac{\partial f_i}{\partial t} + \nabla \cdot (f_i \bar{V}) = 0 \tag{7}$$

$$\sum_{i=1}^{2} f_i = 1 \tag{8}$$

Here $\bar{V}$ is the velocity vector. Eqs (9) & (10) are the density and viscosity of the air-water mixture.

$$\rho = f_i \rho_w + (1 - f_i)\rho_a \tag{9}$$

$$\mu = f_i \mu_w + (1 - f_i)\mu_a \tag{10}$$

Where ρ_w = water density, ρ_a = air density, μ_w = viscosity of water, and μ_a = viscosity of air.

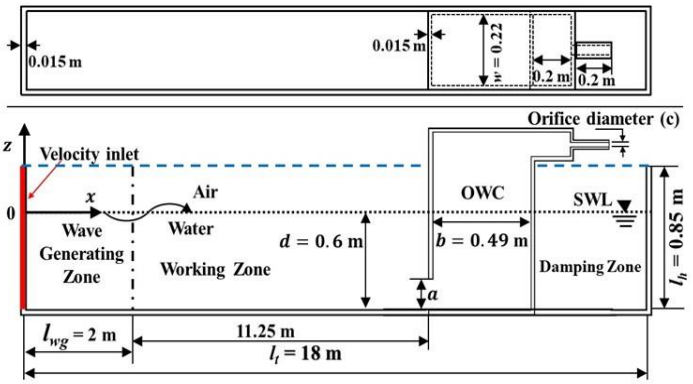

Fig. 1 Definition sketch of the NWT and the OWC devices

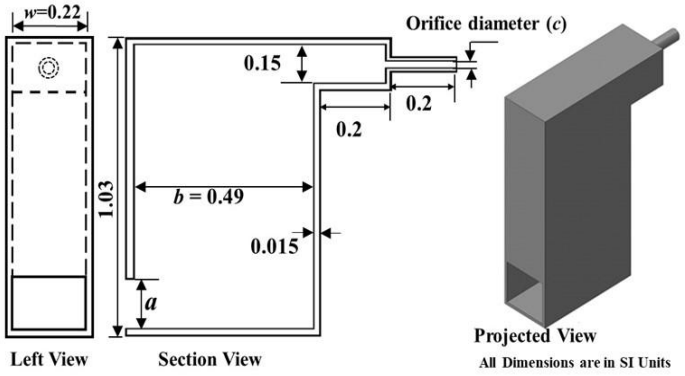

Fig. 2 CAD model of the OWC

Table 1 Geometrical parameters

Orifice ratio (τ)	τ_1= 0.4%	τ_2= 0.58%	τ_3= 0.79%	τ_4= 1.03%	τ_5 = 1.3%
Relative Opening (α)	α_1 = 33%	α_2 = 50%	α_3 = 75%	-	-

3. NUMERICAL MODEL

3.1 Tank Geometry

The sketch of the computational domain of NWT and the OWC devices is exhibited in Fig. 1. The inlet velocity method was used to develop the Second-Order Stokes waves in a numerical wave tank. The waves are propagated in the propagation direction. Tank's upper boundary is open and is connected to the atmosphere, and the right and bottom walls are solid and considered no-slip boundaries. The Cartesian coordinates system is *0xz*. The propagation direction is the *x*-axis, and the vertical axis is the *z*-axis. The normal axis is the *y*-axis and is perpendicular to the *0xz* plane. In Fig. 1, l_h (=0.85m) is the height of the tank, l_{wg} (=2m) is the wave generating zone, l_t (=18m) is the tank length, d (=0.6m) is the depth of water, and a is the chamber's opening height. The waves move along the path of propagation.

3.2 Geometry of the OWC

The OWC model that was employed in this investigation is shown with its geometry in Fig. 2. The model has been designed according to the published model by Çelik and Altunkaynak (2019). 3D CAD software is used to design the OWC energy converter and the dimensions exhibited in Fig. 2. Consider the observation point at the middle point of the OWC chamber. The performance of the OWC is analyzed using the two model parameters, α and τ, as indicated in Table 1.

Orifice Ratio (τ): Orifice cross-sectional area ($S_0 = \frac{\pi}{4}c^2$) and the free surface area ($S_w = b \times w$) inside the OWC chamber; the ratio of the two represents the orifice ratio.

$$\tau = \frac{S_0}{S_w} \tag{11}$$

Relative opening (α): Opening height (a) and the water depth (d); the ratio of the two represents the relative opening.

$$\alpha = \frac{a}{d} \tag{12}$$

The grids, which are rectangular in size, are discretized in the numeral domain. The nodes 330267 on Mesh 3 system (See Table 2) are used for numerical investigation. Based on these nodes, we divide the computational domain into different zones under different values of Δx, Δy, and Δz. The enlarged 3D mesh and OWC model in Fig. 3 help the reader better grasp the numerical approach.

The system specification is Intel(R) Xeon(R) W-2155CPU@3.30GHz 3.31GHz processor and 64.0GB RAM used for the simulation. The system specification is 64.0GB RAM, and the processor is 3.31GHz. The

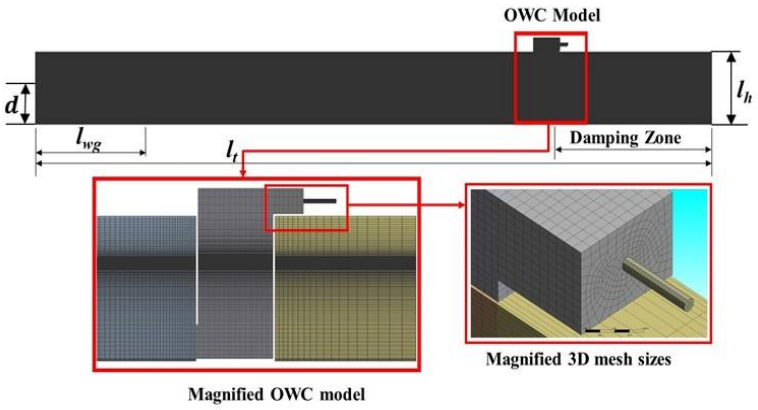

Fig. 3 Computational mesh in the numerical domain

Table 2 Mesh size parameters

Sl. No.	Δ*x* (m)	Δ*y* (m)	Δ*z* (m)	Nodes	Elements
Mesh - 1	0.3600	0.0625	0.0850	109467	91238
Mesh - 2	0.3000	0.0500	0.0566	221076	191977
Mesh - 3	0.2571	0.0275	0.0425	330267	286909
Mesh - 4	0.2250	0.0125	0.0340	420031	381097
Mesh - 5	0.1385	0.0078	0.0190	711112	649280

Raynolds-averaged Navier-Stokes (RANS) equation is discretized. The two schemes used in the process of discretization are: 1) second-order upwind scheme and 2) first-order implicit scheme. The program has selected 0.01s for time steps and 2500 for the size of step time. Iteration selects 30 for the solution. In order to maintain stability, the Courant number = 0.25. It took a total of 26 hours to finish the simulation.

The OWC's hydrodynamic efficiency energy converter is available at the orifice and used to produce electrical power via the prime mover. The pneumatic output power's ratio (P_{out}) created in the orifice to the incoming wave power (P_{in}) is used to compute hydrodynamic efficiency (η). The formula for this calculation is as follows:

$$\eta = \frac{P_{out}}{P_{in}\, w} \tag{13}$$

Where OWC mouth width is *w*.

The average power (P_{out}) from a pneumatic system is calculated as the product of the pressure $p(t)$ in the chamber and the air volume flow rate $S_w v(t)$ as follows:

$$P_{out} = \frac{1}{T}\int_0^T p(t) S_w v(t) dt \tag{14}$$

Where $p(t)$, $v(t)$, S_w, and T are the usual meaning as given in nomenclature.

The incident wave power (P_{in}) is calculated using second-order Stokes wave theory per unit width, as shown in the following equation (Boualia and Larbib (2013).

$$P_{in} = \frac{1}{8}\rho g H^2 \frac{\omega}{k}\left[\frac{1}{2}\left(1+\frac{2kd}{\sinh(2kd)}\right)\right]\left[1+\frac{9H^2}{64k^4d^6}\right] \tag{15}$$

Where *H, ω, k,* and *d* are the usual meaning as given in nomenclature.

3.3 Convergent Test

Table 2 exhibited Mesh 1, Mesh 2, Mesh 3, Mesh 4, and Mesh 5, and the size of the meshes decreased bit by bit. Corresponding nodules are 109467, 221076, 330267, 420031, and 711112 of the five mashes. Figure 4 shows pressure vs. time (*t*) graphs to compare the mesh systems. The observation of the results shows no such variation among Mesh 3, Mesh 4, and Mesh 5. Because of this, the Mesh 3 system is used for every numerical simulation. Here, the observation point is (13.51,0.4) at the middle point of the OWC device.

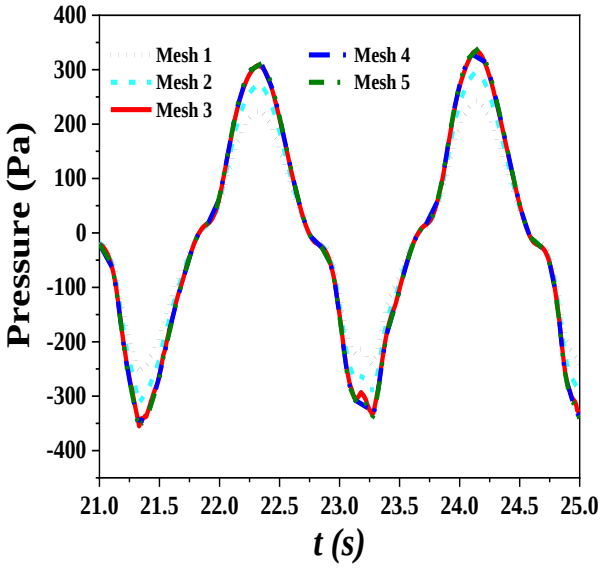

Fig. 4 Pressure versus Time (*t*) at *H/L* =0.02, *α* = 75%, and *τ* = 1.03%

Table 3 Wave parameters

Sl. No.	Wave Height (H)m	Wave Length (L)m	Time Period (T)sec	Wave Steepness (H/L)	Relative depth (d/L)
	0.07	3.8548	1.812	0.02	0.1556
2	0.08	2.7699	1.427	0.03	0.2166
3	0.09	2.2041	1.236	0.04	0.2722
5	0.10	2.0019	1.168	0.05	0.2997
4	0.11	2.2738	1.26	0.045	0.2639

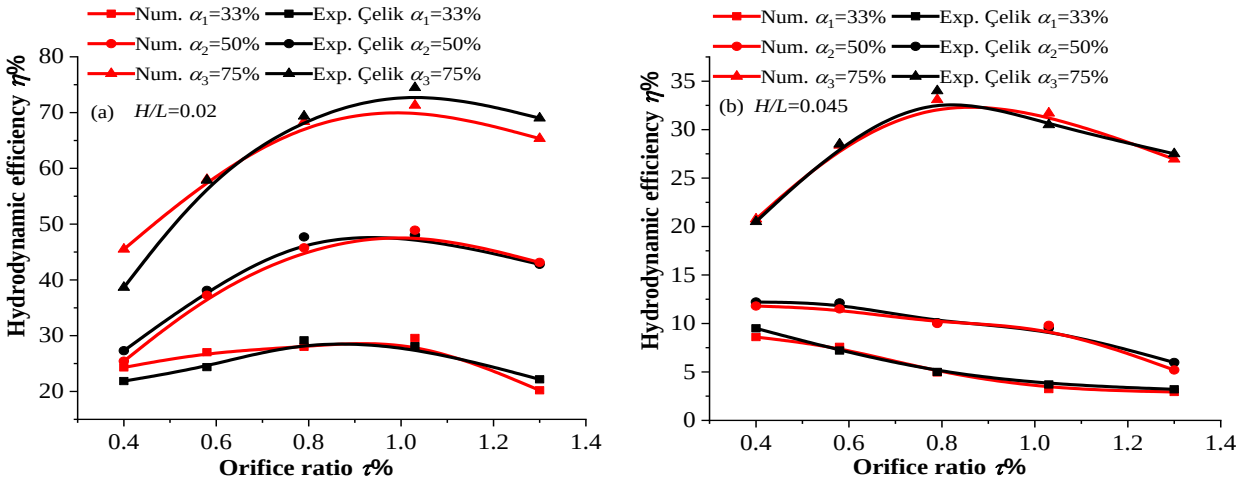

Fig. 5 Hydrodynamic efficiency (η) versus orifice ratio (τ) in comparison with the present numerical model and published experimental model (Celik and Altunkaynak 2019) at (a) H/L = 0.02 and (b) H/L = 0.045

3.4 Validation of the Model

The published experimental model of flat-bottom OWC presented in Çelik and Altunkaynak (2019) has been the basis for validating and verifying the current numerical model. During validation, we considered the width of the numerical OWC device to be the same as that of the width of the wave tank, and the dimensions and other wave parameters have been kept the same as in the experimental model. The static water depth is 0.60m. Two wave steepnesses (H/L = 0.02 and 0.045) and three relative openings (α = 33%, 50%, and 75%) are considered for the validation. Table 3 exhibits the wave parameters that were employed in this model. It has been observed from Fig. 5 the proposed model is in good acceptance with the published investigative model. It has also been shown that the basic geometry of each efficiency curve agrees adequately between itself for each value of relative opening (α). Overall, the proposed numerical model matches satisfactorily with the experimental model. A maximal approximate error of 3.88% and a minimal approximate error of 0.14% were found for H/L = 0.02. Similarly, the maximal approximate error is 2.10%, and the minimal approximate error is 0.06% for H/L = 0.045. Therefore, the present numerical model is approved and appropriate, and we can investigate further.

4. RESULTS AND DISCUSSION

4.1 Effect of Orifice Ratio

Turbine damping appears in the two extreme cases. The first one is zero orifice diameters, i.e., very high damping. The water velocity $v(t)$ is zero within the chamber. And the second one is a very large orifice diameter, i.e., the pressure $p(t)$ inside the chamber is zero. Accordingly, Eq. (14) will be zero in both cases. Therefore, to extract the maximum wave energy from the incident wave, it is required to optimize the orifice size so that the product of air pressure and water velocity becomes maximum.

The hydrodynamic efficiencies corresponding to the orifice ratio are shown in Figs. 6 to 10 for different values of relative opening (α = 33%, 50%, and 75%) and H/L =0.02, 0.03, 0.04, 0.045, and 0.05. The concave shape of all graphs has shown in Fig. 6, and the efficiency (η) of OWC reaches its maximum value at α = 75%. This has also been observed: for all relative openings, the lowest orifice ratio produced poor efficiency, as shown in Fig. 6. Very high air pressure is generated due to the damping effect inside the OWC at the smallest orifice diameter, and the free surface motion of water within the OWC is low. Therefore, less power is extracted. When the τ rises, the OWC's efficiency rises at first but drops off gradually. The maximum adaptability is always obtained at τ_4 = 1.03% for H/L = 0.02. This orifice ratio gives the optimal damping to obtain the maximum efficiency at H/L = 0.02.

Figure 7 shows at H/L = 0.03 between hydrodynamic efficiency vs orifice ratio. It has been observed that hydrodynamic efficiency (η) decreases linearly with the increase of orifice ratio (τ) for the relative opening α_1 = 33%, and it gives maximum efficiency at τ_1 = 0.40%. Figure 7 shows that the shape of the graph is concave for relative opening α_2 = 50% and α_3 = 75%. The efficiency shows the maximum values at the orifice ratio τ_2 = 0.58% for α_2 and τ_3 = 0.79% for α_3. The explanation reveals that

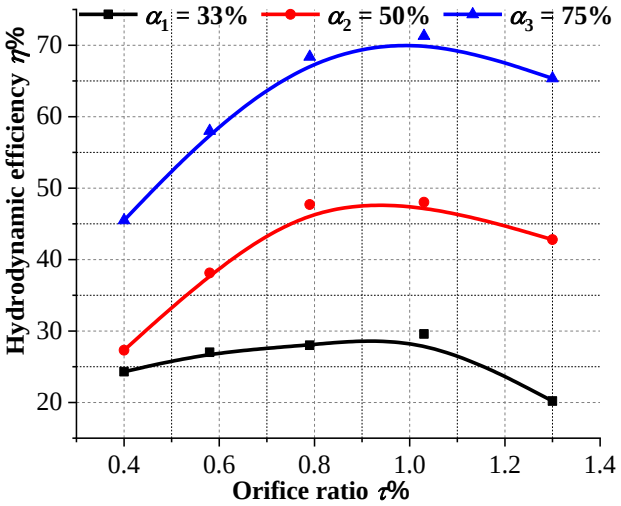

Fig. 6 Hydrodynamic efficiency v/s orifice ratio (τ) for *H/L* = 0.02

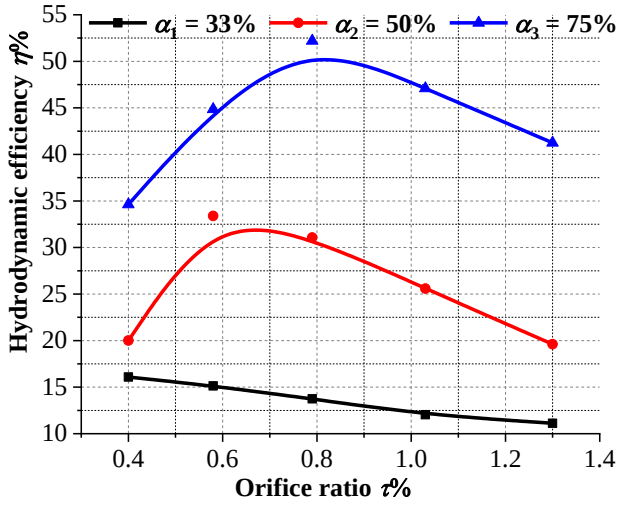

Fig. 7 Hydrodynamic efficiency v/s orifice ratio (τ) for *H/L* = 0.03

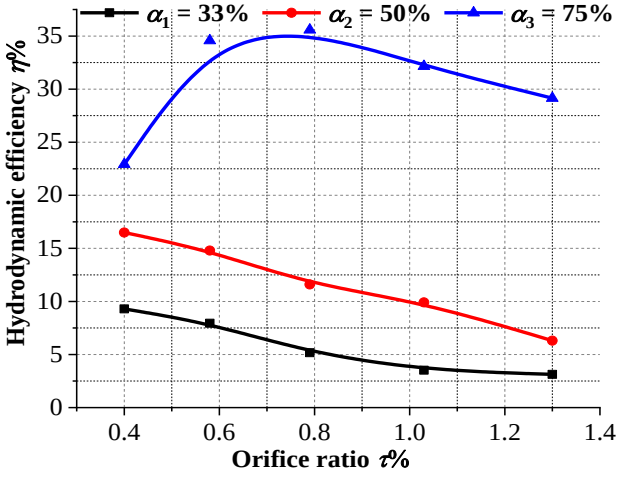

Fig. 8 Hydrodynamic efficiency v/s orifice ratio (τ) for *H/L* = 0.04

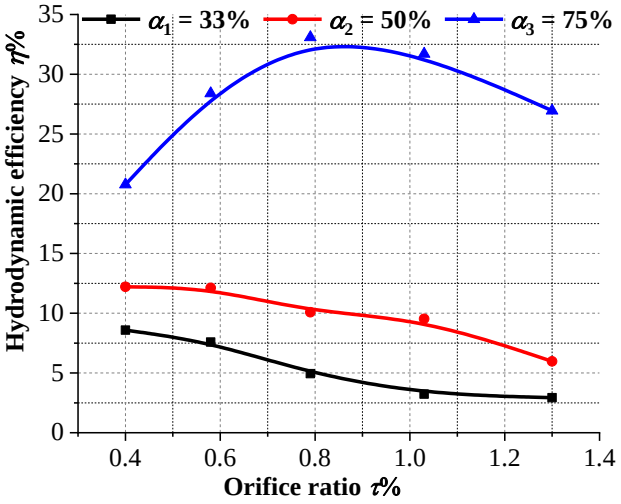

Fig. 9 Hydrodynamic efficiency v/s orifice ratio (τ) for *H/L* = 0.045

the optimal damping of the system at *H/L* = 0.03 is different compared to the previous description.

Figure 8 illustrates the graphs at *H/L* =0.04. It has been observed that hydrodynamic efficiency (η) decreases linearly with the increase of orifice ratio (τ) for the relative opening α_1 = 33% and α_2 = 50%, and a concave shape is observed for the relative opening α_3 = 75%. The efficiency shows a maximum value at the orifice ratio τ_3 = 0.79% for α_3.

The illustration of hydrodynamic efficiency (η) of Fig. 9 and Fig. 8 are the same. The performance of the energy converter is maximum for α_1 and α_2 at τ_1 = 0.40%. The performance of the energy converter increases with the increase of office ratio (τ) and then decreases for the relative opening α_3 = 75%. The efficiency shows the maximum value for α_3 at the orifice ratio τ_3 = 0.79%. It has been observed from the above discussion that the performance of the energy converter follows the same trend as *H/L* = 0.04 and 0.45.

Figure 10 shows the highest performance at τ_1 = 0.40% for all relative openings (α). It has been demonstrated that efficiency (η) decreases linearly for all relative openings (α). The above discussion from Figs. 6

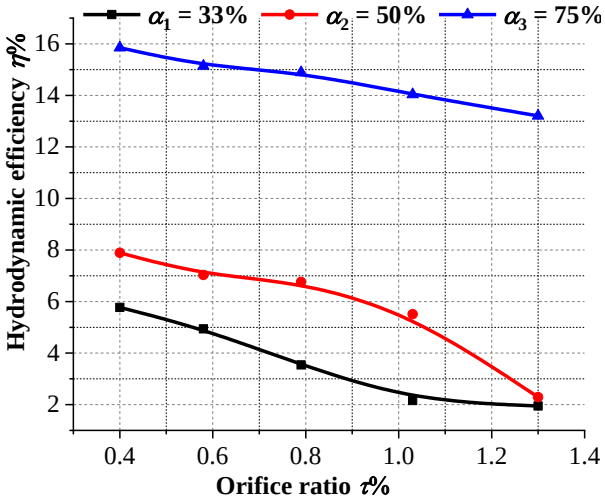

Fig. 10 Hydrodynamic efficiency v/s orifice ratio (τ) for *H/L* = 0.05

to 10 shows that the efficiency (η) depends on *H/L*. It has been observed that hydrodynamic efficiency (η) gives the best result for (*H/L*) = 0.02 in comparison to others (*H/L* = 0.03, 0.04, 0.045, and 0.05). It has also been observed that the performance of OWC gives the optimal at τ_4 =

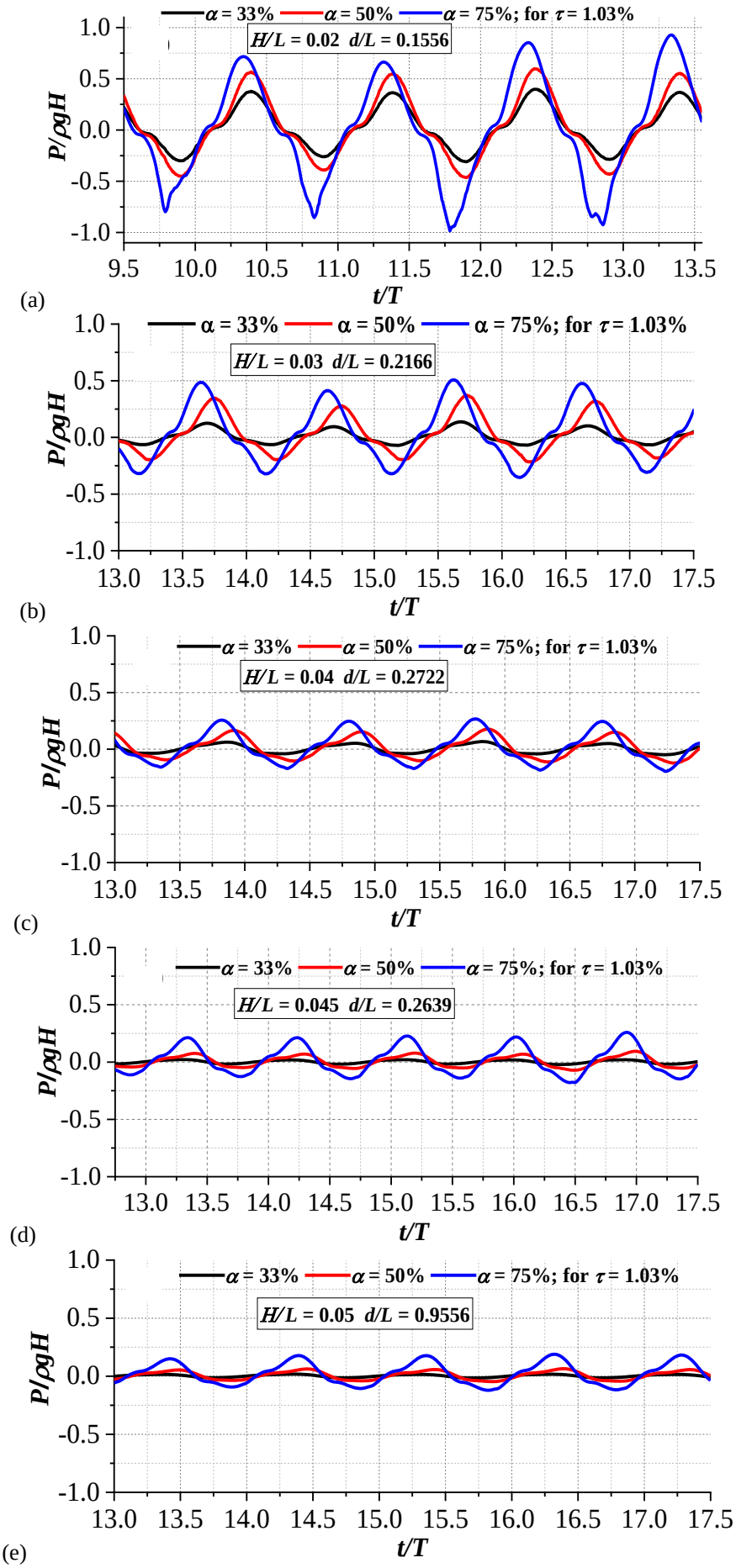

Fig. 11(a-e). Non-dimensional air pressure *P/ρgH* versus time *t/T* at different relative openings (*α*) and constant orifice ratio *τ* = 1.03%

1.03% and α_3 = 75%. Due to this, the steeper incident waves need significantly stronger damping to achieve the greatest possible hydrodynamic performance.

4.2 Wave Steepness's Effect on Air Pressure

With a constant orifice ratio (τ) of 1.03%, the air pressure effected within the chamber by the wave steepness at various relative openings (α = 33%, 50%, and 75%) is shown in Fig. 11. In all cases, air pressure is measured near the orifice, and the graphs are periodic.

Optimal power is obtained at (H/L) = 0.02 and an orifice ratio τ = 1.03%. Air pressure reduces as the wave steepness increases, and at H/L = 0.05, the pressure is very low for the relative openings, α = 33%. It has been shown in the figures that the air pressure increases with a decrease in wave steepness (H/L). It has shown in Fig. 11(a) that the air pressure reaches a maximum value at d/L = 0.1556 and H/L = 0.02 for α = 75%. It has also shown that the pressure of the air inside the OWC energy converter is greater at α = 75% and lower at α = 33% for all steepness of waves. The lower air pressure for α = 33% because of the wave reflection due to the OWC's lip wall would significantly take vortex development on its lip side. This phenomenon reduces the energy converter's performance due to the water level reduction within the chamber.

4.3 Effect of Relative Opening

The relative opening is an important study in the performance of the OWC. Figures 12 to 16 illustrate the performance of hydrodynamic efficiency (η) of the OWC versus α (relative openings) under different steepness of wave (H/L) and τ (orifice ratio). Under various steepness of wave (H/L) conditions, as shown in Figs. 12–16, efficiency rises with relative openings for all values of orifice ratios. The efficiencies show a maximum for H/L = 0.02 compared to other steepness. For every given wave steepness, it has been noticed that the efficiency is at its best when α_3 = 75% and that lowest when α_1 = 33%. According to the definition of relative opening, the height of the front wall is small for α_3 = 75% and maximum for α_1 = 33%. Therefore, the wave reflection of the incident wave is low due to the small height of the front wall as compared to the maximum height of the front wall. Figure 12 shows the lowest efficiency for all values of relative openings (α) at τ_1 = 0.40%. Figure 12 illustrates the greatest efficiency achieved when the τ = 1.03%.

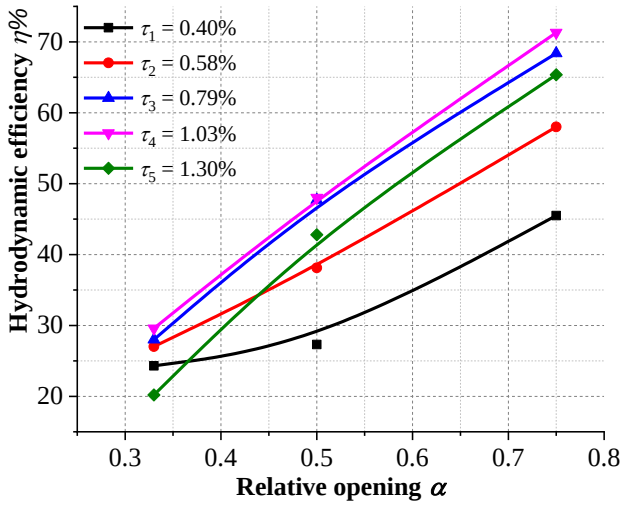

Fig. 12 Hydrodynamic efficiency v/s relative opening (α) for H/L = 0.02

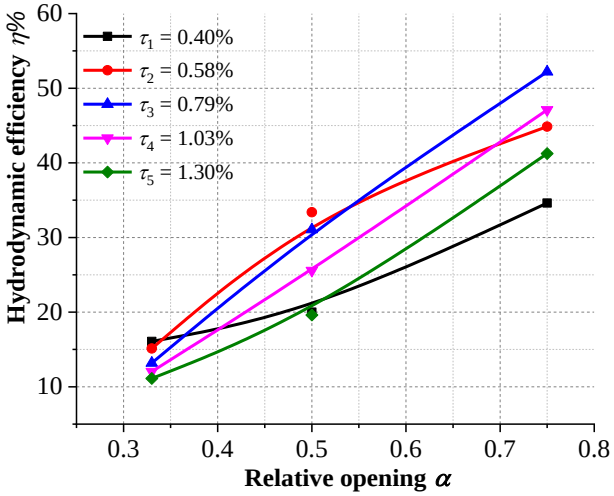

Fig. 13 Hydrodynamic efficiency v/s relative opening (α) for H/L = 0.03

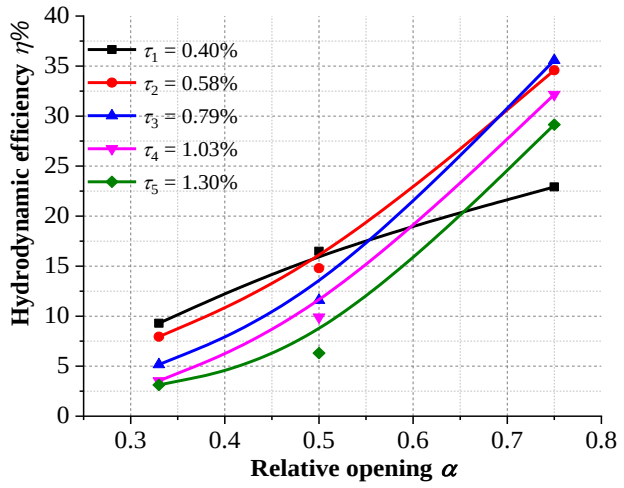

Fig. 14 Hydrodynamic efficiency v/s relative opening (α) for H/L = 0.04

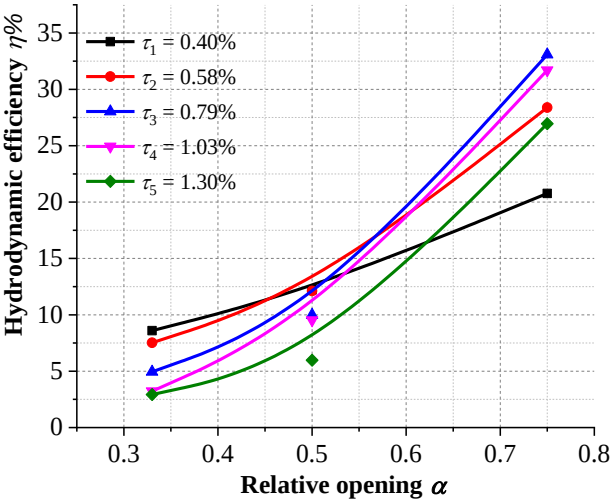

Fig. 15 Hydrodynamic efficiency v/s relative opening (α) for H/L = 0.045

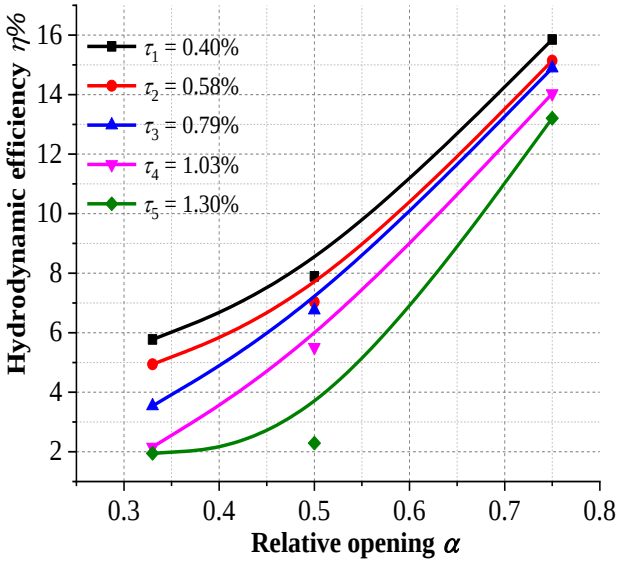

Fig. 16 Hydrodynamic efficiency v/s relative opening (α) for H/L = 0.05

4.4 Effect of Wave Steepness

Figure 17 shows the plot of energy converter efficiency (η) v/s steepness of wave (H/L) under different α (relative opening) and τ (orifice ratios). Energy efficiency (η) is significantly influenced by the steepness of the wave (H/L). The performance of OWC linearly decreases with the increases in wave steepness shown in Fig. 17. For all values of α, it has also been shown that the efficiency is prominent at H/L = 0.02. Figure 17(c) also shows that the energy efficiency gradually converged at H/L = 0.05. for α = 75%.

4.5 Streamline Study

The streamlines and the free surface motion of the wave near the lip wall and in the vertical column of the OWC are required for further study to understand the wave steepness's (H/L) effect on the efficiency at two different relative openings (α) of 33% and 75%. This study is based on one wave cycle during which the wave completes the inhalation and exhalation of air through the orifice.

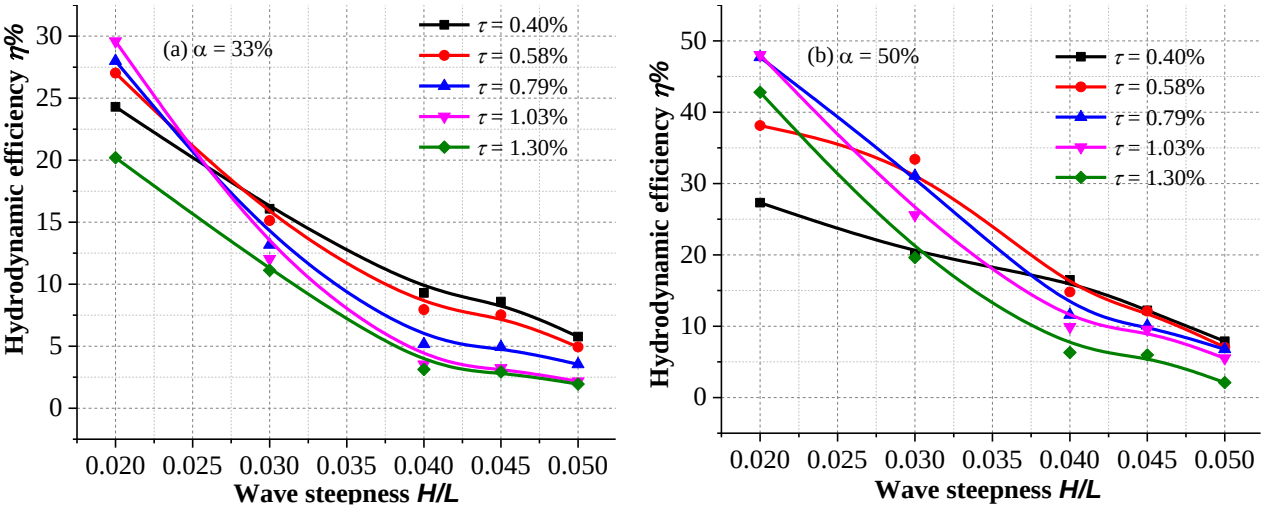

Fig. 17(a-b) Hydrodynamic efficiency v/s H/L for different relative opening

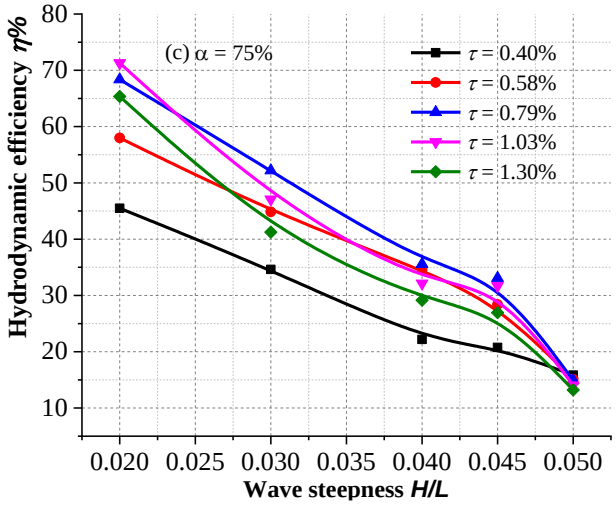

Fig. 17(c) Hydrodynamic efficiency v/s H/L for different relative opening

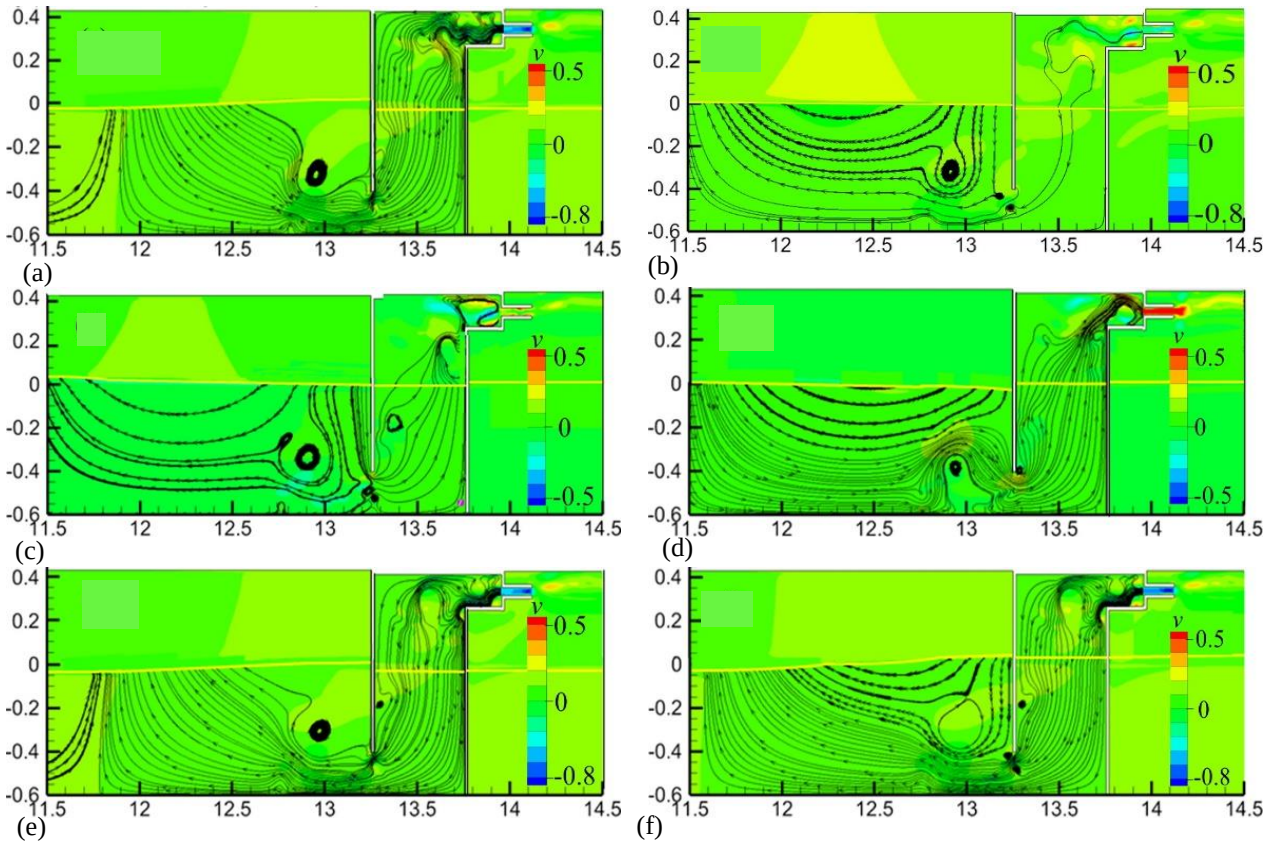

Fig. 18 Streamlines and free surface motions near the device and within the chamber for *H/L*=0.02 and *α* = 33% based on one wave cycle. (a) *t/T*=12.48, (b) *t/T*=12.70, (c) *t/T*=12.81, (d) *t/T*=13.09, (e) *t/T*=13.48, (f) *t/T*=13.53

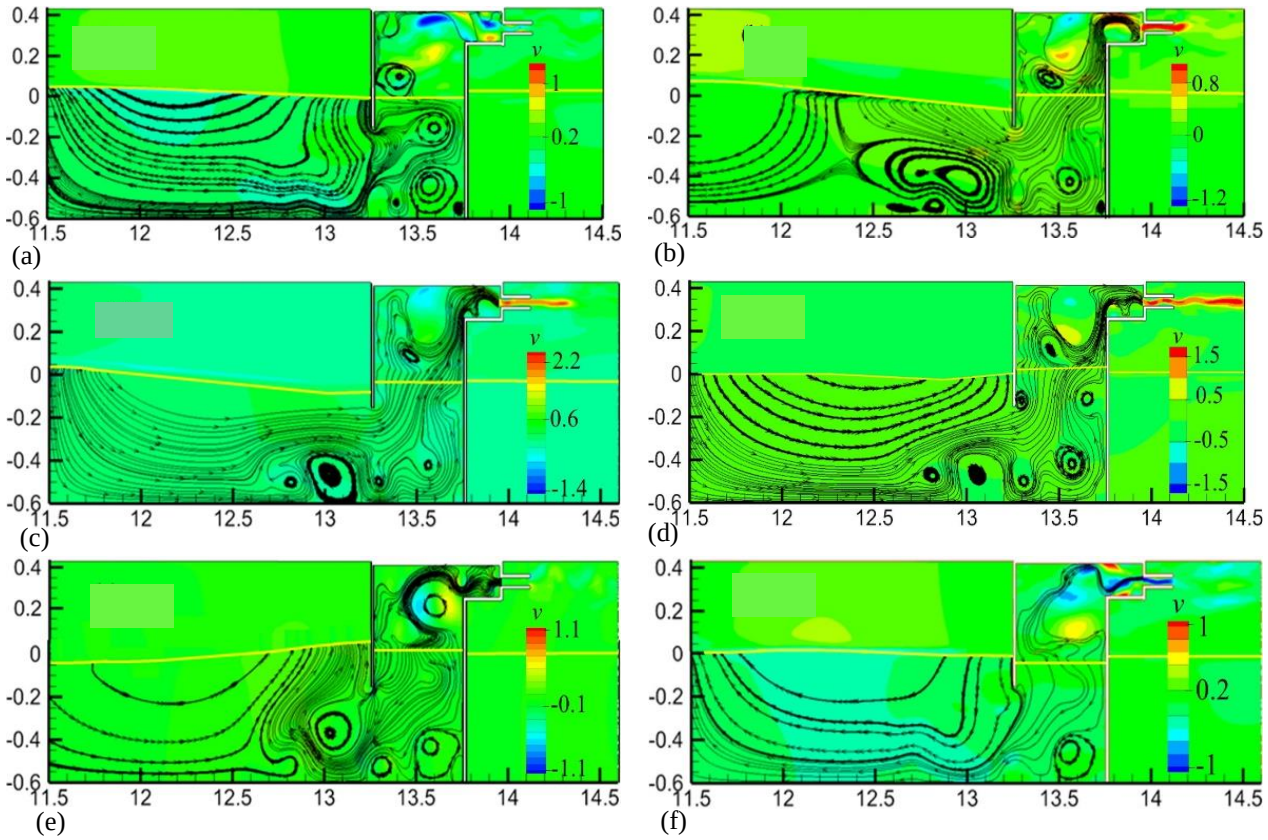

Fig. 19 Streamlines and free surface motions near the device and within the chamber for *H/L*=0.02 and *α* = 75% based on one wave cycle. (a) *t/T*=12.76, (b) *t/T*=12.92, (c) *t/T*=13.03, (d) *t/T*=13.14, (e) *t/T*=13.37, (f) *t/T*=13.70

Figure 18 shows the waves' streamlined motion and free surface motion for H/L = 0.02 at a relative opening, α = 33%. It has been observed in Fig. 18(a) that the inhalation process just starts and is completed in Fig. 18(b), and the free surface's motion shows at the lowest elevation. After that, the exhalation of air pressure starts in Fig. 18(c), showing that the free surface is moving upward uniformly. It has also been noticed that vortex formation starts at the lip wall, indicating that the water is trying to move into the chamber. Figure 18(d) shows that after the completion of exhalation, the free surface motion is maximum, and the water surface reaches its top level. It shows the inhalation phase in Fig. 18(e & f), and the trend of free surface motion uniformly moves downwards. Each figure shows the vortex formation at the opening of the front wall due to low relative opening α = 33%, indicating a low volume of flux entering the chamber. Due to this hydrodynamic performance of OWC reduces. No such vortex formation was observed at the inside of the back wall.

Figure 19 shows the water level movement in the inside vacuum space of the OWC converter and the streamlined motion for one wave at H/L = 0.02, α = 75%. It has shown in Fig. 19(a) that the inhalation process was completed and showed the free surface motion at the lowest elevation. The vortex formation is shown at the opening of the front wall. And also at the back wall inside the chamber. This indicates that water is rushing out from the chamber to the NWT. After that, it has shown in Fig. 19(b) that the exhalation of air pressure just starts, and the free surface uniformly moves upwards in the chamber. Figure 19(d) shows that at the end of exhalation, the free surface motion is maximum, and the water surface reaches its maximum level. The vortex formation is shown in Fig. 19(b, c & d), indicating incident wave energy entering into the chamber. After that, the inhalation phase started at time t/T =13.37, shown in Fig. 19(e), and has completed at time t/T =13.70, shown in Fig. 19(f). The above explanation shows that the volume of flux entering the chamber is more predominant at a relative opening α = 75% compared to the lower α = 33% at H/L = 0.02 and orifice ratio τ = 1.03% resulting in a higher power absorption by the device. Therefore, optimal efficiency obtained at a α = 75%, H/L = 0.02, and orifice ratio τ = 1.03%.

5. CONCLUSION

The performance of the rectangular-based OWC model has been assessed through numerical investigation in a nonlinear wave field. Variations in relative opening and orifice ratio are taken into consideration for the study of the performance of OWC devices. The results of the promulgated experimental model that Çelik and Altunkaynak (2019) have described in their experimental work are compared with the results of the current numerical analysis. To understand the performance of the present OWC energy converter, we have considered 3-α (relative openings) and 5-τ (orifice ratios).-Hydrodynamic efficiency, water column velocity, and pressure are essential studies in this problem. The following points are concluded from the above study:

1. The energy (η) of the present numerical model is affected by τ (orifice ratios), α (relative opening), and H/L (steepness of wave).
2. The energy (η) of the present model varies, corresponding to the variation of orifice ratios (τ). A maximum value of efficiency (η) is achieved between orifice ratios (τ) = 0.79% to 1.03% for all α (relative opening). Maximum energy of around 71.3% is achieved in this numerical work at τ = 1.03%, α = 75%, and H/L = 0.02.
3. For each given value of the wave steepness (H/L), an increase in the relative openness (α) improves the hydrodynamic efficiency (η). The maximum efficiency is obtained at H/L = 0.02, α =75%, and τ = 1.03% because the wave is reflected in a very low amount.
4. The efficiency (η) decays in all cases with the increases in wave steepness (H/L). 71.3% is the maximal efficiency achieved at τ (orifice ratio) = 1.03%, H/L (wave steepness) = 0.02, and α (relative opening) = 75%.

ACKNOWLEDGMENTS

I am grateful to the Department of Mechanical Engineering, NIT Silchar, Assam, for helping me to develop the simulation laboratory.

CONFLICT OF INTEREST

The authors have no conflicts to disclose.

AUTHORS CONTRIBUTION

In this work, both authors have more or less the same role. I have developed the idea and mathematical coding and analyzed the overall results. I have written the whole manuscript logically. My student solves the problem numerically using CFD code Ansys Fluent software and draws all graphs under my supervision. He also validated the numerical results with the published experimental results. I have taken oversight and leadership responsibility for the research activity planning and execution.

REFERENCES

Ashlin, S. J., Sundar, V., & Sannasiraj, S. A. (2016). Effects of bottom profile of an oscillating water column device on its hydrodynamic characteristics. *Renewable Energy*, 96, 341-353. https://doi.org/10.1016/j.renene.2016.04.091

Bouali, B., & Larbi, S. (2013). Contribution to the geometry optimisation of an oscillating water column wave energy converter. *Energy Procedia*, 36, 565-573. https://doi.org/10.1016/j.egypro.2013.07.065

Çelik, A., & Altunkaynak, A. (2019). Experimental investigations on the performance of a fixed-oscillating water column type wave energy

converter. *Energy*, 188, 116071. https://doi.org/10.1016/j.energy.2019.116071

Count, B. M., & Evans, D. V. (1984). The influence of projecting sidewalls on the hydrodynamic performance of wave-energy devices. *Journal of Fluid Mechanics*, 145, 361-376. https://doi.org/10.1017/S0022112084002962

Delauré, Y. M. C., & Lewis, A. (2003). 3D hydrodynamic modelling of fixed oscillating water column wave power plant by a boundary element methods. *Ocean Engineering*, 30(3), 309-330. https://doi.org/10.1016/S0029-8018(02)00032X

Dizadji, N., & Sajadian, S. E. (2011). Modeling and optimization of the chamber of OWC system. *Energy*, 36(5), 2360-2366. https://doi.org/10.1016/j.energy.2011.01.010

El Marjani, A., Ruiz, F. C., Rodriguez, M. A., & Santos, M. P. (2008). Numerical modelling in wave energy conversion systems. *Energy*, 33(8), 1246-1253. https://doi.org/10.1016/j.energy.2008.02.018

Evans, D. V. (1978). The oscillating water column wave-energy device. *IMA Journal of Applied Mathematics*, *22*(4), 423-433. https://doi.org/10.1093/imamat/22.4.423

Evans, D. V. (1982). Wave-power absorption by systems of oscillating surface pressure distributions. *Journal of Fluid Mechanics*, 114, 481-499. https://doi.org/10.1017/S0022112082000263

Evans, D. V., & Porter, R. (1995). Hydrodynamic characteristics of an oscillating water column device. *Applied Ocean Research*, 17(3), 155-164. https://doi.org/10.1016/0141-1187(95)00008-9

Falcão, A. D. O., & Sarmento, A. J. N. A. (1980, August). *Wave generation by a periodic surface pressure and its application in wave-energy extraction*. 15th International Congress of Theoritical and Applied Mechanics. (ICTAM), Toronto.

Falcão, A. F., & Henriques, J. C. (2016). Oscillating-water-column wave energy converters and air turbines: A review. *Renewable Energy*, 85, 1391-1424. https://doi.org/10.1016/j.renene.2015.07.086

Falnes, J., & McIver, P. (1985). Surface wave interactions with systems of oscillating bodies and pressure distributions. *Applied Ocean Research*, 7(4), 225-234. https://doi.org/10.1016/0141-1187(85)90029-X

Gouaud, F., Rey, V., Piazzola, J., & Van Hooff, R. (2010). Experimental study of the hydrodynamic performance of an onshore wave power device in the presence of an underwater mound. *Coastal Engineering*, 57(11-12), 996-1005. https://doi.org/10.1016/j.coastaleng.2010.06.003

Hirt, C. W., & Nichols, B. D. (1981). Volume of fluid (VOF) method for the dynamics of free boundaries. *Journal of Computational Physics*, 39(1), 201-225. https://doi.org/10.1016/0021-9991(81)90145-5

Hotta, H., Miyazaki, T., Washio, Y., & Ishii, S. (1988). *On the performance of the wave power device Kaimei—the results on the open sea tests*. Proceedings of the Seventh International Conference on Offshore Mechanics and Arctic Engineering, Houston, TX, USA.

Iturrioz, A., Guanche, R., Lara, J. L., Vidal, C., & Losada, I. J. (2015). Validation of OpenFOAM® for oscillating water column three-dimensional modeling. *Ocean Engineering*, 107, 222-236. https://doi.org/10.1016/j.oceaneng.2015.07.051

Josset, C., & Clément, A. H. (2007). A time-domain numerical simulator for oscillating water column wave power plants. *Renewable Energy*, 32(8), 1379-1402. https://doi.org/10.1016/j.renene.2006.04.016

Liu, Z. 2008. *Experimental and numerical investigation of oscillating water column wave energy convertor*. [Doctoral Thesis, Qingdao, Ocean University of China].

Liu, Z., Hyun, B., Jin, J., Hong, K., & Lee, Y. (2016). OWC air chamber performance prediction under impulse turbine damping effects. *Science China Technological Sciences*, 59, 657-666. https://doi.org/10.1007/s11431-016-6030-5

López, I., Pereiras, B., Castro, F., & Iglesias, G. (2014). Optimisation of turbine-induced damping for an OWC wave energy converter using a RANS–VOF numerical model. *Applied Energy*, 127, 105-114. https://doi.org/10.1016/j.apenergy.2014.04.020

Luo, Y., Nader, J. R., Cooper, P., & Zhu, S. P. (2014). Nonlinear 2D analysis of the efficiency of fixed oscillating water column wave energy converters. *Renewable Energy*, 64, 255-265. https://doi.org/10.1016/j.renene.2013.11.007

Malmo, O., & Reitan, A. (1985). Wave-power absorption by an oscillating water column in a channel. *Journal of Fluid Mechanics*, 158, 153-175. https://doi.org/10.1017/S0022112085002592

Malmo, O., & Reitan, A. (1986). Wave-power absorption by an oscillating water column in a reflecting wall. *Applied Ocean Research, (United Kingdom)*, 8(1). https://doi.org/10.1016/S0141-1187(86)80030-X

McCormick, M. E. (1976). A modified linear analysis of a wave-energy conversion buoy. *Ocean Engineering*, 3(3), 133-144. https://doi.org/10.1016/0029-8018(76)90029-9

Mccormick, M. E., & Burcher, E. S. (1982*). Pneumatic wave energy conversion*. Energy Resources and Environment, Pergamon. https://doi.org/10.1016/B978-0-08-029396-7.50047-1

Mork, G., Barstow, S., Kabuth, A., & Pontes, M. T. (2010, January). *Assessing the global wave energy potential*. International Conference on Offshore Mechanics and Arctic Engineering . https://doi.org/10.1115/OMAE2010-20473

Morris-Thomas, M. T., Irvin, R. J., & Thiagarajan, K. P. (2007). *An investigation into the hydrodynamic*

efficiency of an oscillating water column. https://doi.org/10.1115/1.2426992

Nagata, S., Imai, Y., Murakami, T., & Okamoto, Y. (2017, June 25-30). *Numerical analysis on drift force acting on a floating OWC-type wave energy converter "backward bent duct buoy" by vortex method.* ISOPE International Ocean and Polar Engineering Conference ISOPE. San Francisco, California, USA.

Ning, D. Z., Shi, J., Zou, Q. P., & Teng, B. (2015). Investigation of hydrodynamic performance of an OWC (oscillating water column) wave energy device using a fully nonlinear HOBEM (higher-order boundary element method). *Energy*, 83, 177-188. https://doi.org/10.1016/j.energy.2015.02.012

Ning, D. Z., Wang, R. Q., Zou, Q. P., & Teng, B. (2016a). An experimental investigation of hydrodynamics of a fixed OWC Wave Energy Converter. *Applied Energy*, 168, 636-648. https://doi.org/10.1016/j.apenergy.2016.01.107

Ning, D. Z., Wang, R. Q., Gou, Y., Zhao, M., & Teng, B. (2016b). Numerical and experimental investigation of wave dynamics on a land-fixed OWC device. *Energy*, 115, 326-337. https://doi.org/10.1016/j.energy.2016.09.001

Pereiras, B., López, I., Castro, F., & Iglesias, G. (2015). Non-dimensional analysis for matching an impulse turbine to an OWC (oscillating water column) with an optimum energy transfer. *Energy*, 87, 481-489. https://doi.org/10.1016/j.energy.2015.05.018

Pinson, P., Reikard, G., & Bidlot, J. R. (2012). Probabilistic forecasting of the wave energy flux. *Applied Energy*, 93, 364-370. https://doi.org/10.1016/j.apenergy.2011.12.040

Pontes, M. T., & Falcao, A. N. T. Ó. N. I. O. (2001, October). *Ocean energies: resources and utilisation. world energy council*. 18th Congress, Buenos Aires.

Simonetti, I., Cappietti, L., Elsafti, H., & Oumeraci, H. (2017). Optimization of the geometry and the turbine induced damping for fixed detached and asymmetric OWC devices: A numerical study. *Energy*, 139, 1197-1209. https://doi.org/10.1016/j.energy.2017.08.033

Thiruvenkatasamy, K., & Neelamani, S. (1997). On the efficiency of wave energy caissons in array. *Applied Ocean Research*, 19(1), 61-72. https://doi.org/10.1016/S0141-1187(97)00008-4

Tseng, R. S., Wu, R. H., & Huang, C. C. (2000). Model study of a shoreline wave-power system. *Ocean Engineering*, 27(8), 801-821. https://doi.org/10.1016/S0029-8018(99)00028-1

Wang, D. J., Katory, M., & Li, Y. S. (2002). Analytical and experimental investigation on the hydrodynamic performance of onshore wave-power devices. *Ocean Engineering*, 29(8), 871-885. https://doi.org/10.1016/S0029-8018(01)00058-0

Washio, Y., Osawa, H., Nagata, Y., Furuyama, H., & Fujita, T. (2000). *The offshore floating type wave power device 'Mighty Whale': open sea tests.* Proceedings of the 10 International Offshore and Polar Engineering Conference, 373–380, Seattle, USA.

Whittaker, T. J. T., & Stewart, T. P. (1993, July*). An experimental study of nearshore and shoreline oscillating water columns with harbours*. European Wave Energy Symposium.

Whittaker, T. J. T., McIlwaine, S. J., & Raghunathan, S. (1993, July). *A review of the Islay shoreline wave power station*. Proceedings of First European Wave Energy Symposium.

Yadav, S. S., & DebRoy, P. (2022). Generation of stable linear waves in shallow water in a Numerical wave tank. *Journal of Applied Fluid Mechanics*, 15(2), 537-549. https://doi.org/10.47176/jafm.15.02.32987

Yu, Z., Ye, J., & You, Y. (1997). *Site test of a 20kW wave power station at Dawashan Island*. 16th International Conference on Offshore Mechanics and Arctic Engineering vol. 1- B, 97 104, Yokohama, Japan.

Zhang, Y., Zou, Q. P., & Greaves, D. (2012). Air–water two-phase flow modelling of hydrodynamic performance of an oscillating water column device. *Renewable Energy*, 41, 159-170. https://doi.org/10.1016/j.renene.2011.10.011